Since January 2020 Elsevier has created a COVID-19 resource centre with free information in English and Mandarin on the novel coronavirus COVID-19. The COVID-19 resource centre is hosted on Elsevier Connect, the company's public news and information website.

Biosensors and Bioelectronics 202 (2022) 113981

Contents lists available at ScienceDirect

Biosensors and Bioelectronics

journal homepage: www.elsevier.com/locate/bios

Detection and discrimination of SARS-CoV-2 spike protein-derived peptides using THz metamaterials

Soo Hyun Lee [a,1], Yeon Kyung Lee [a,b,1], Sang-Hun Lee [a,c], Jisung Kwak [a,d], Hyun Seok Song [a,**], Minah Seo [a,e,*]

[a] Sensor System Research Center, Korea Institute of Science and Technology (KIST), Seoul, 02792, Republic of Korea
[b] Department of Biomycrosystem Technology, Korea University, Seoul, 02841, Republic of Korea
[c] Department of Optical Engineering, Kumoh National Institute of Technology, Gumi, Gyeongbuk, 39177, Republic of Korea
[d] Department of Chemical and Biological Engineering, Korea University, Seoul, 02841, Republic of Korea
[e] KU-KIST Graduate School of Converging Science and Technology, Korea University, Seoul, 02841, Republic of Korea

ARTICLE INFO

Keywords:
SARS-CoV molecular sensing
Severe acute respiratory syndrome family
Terahertz time-domain spectroscopy
Metamaterials

ABSTRACT

The development of effective assay techniques for severe acute respiratory syndrome coronavirus 2 (SARS-CoV-2) has recently received research attention due to its rapid worldwide spread and considerable risk to human health. The receptor-binding domain (RBD) of the spike (S) protein in SARS-CoV-2, a key component for viral entry that has a unique sequence compared to other structural proteins, has been considered an important diagnostic target. In this respect, low-frequency vibrational modes have the advantage of providing information about compositional and structural dependencies at the peptide level. In this study, the sensitive and selective detection of peptides derived from the RBD in SARS-CoV-2 and SARS-CoV was investigated using metamaterial-based sensing chips with a terahertz time-domain spectroscopy (THz-TDS) system. Based on their RBD sequences, two pairs of peptides with 20 residues each were prepared. The sensitivity, specificity, and reproducibility of the proposed system were examined *via* quantitative analysis using THz metamaterials at three resonance frequencies, and it was found that the species could be discriminated based on their sequences. The THz signals were analyzed with regard to the major amino acid components of the peptides, and the molecular distributions were also investigated based on the hydropathy and net charge of the peptides.

1. Introduction

The novel coronavirus disease 2019 (COVID-19), caused by the severe acute respiratory syndrome coronavirus 2 (SARS-CoV-2) and first reported in Wuhan, China, in December 2019, remains a significant threat to public health globally (Zhu et al., 2020; Wang et al., 2020; Sun et al., 2020). Within three months of its emergence, the World Health Organization declared the COVID-19 to be a pandemic. The rapid global spread of COVID-19 is due to several factors. In particular, SARS-CoV-2 predominantly spreads through human-to-human transmission *via* the inhalation of contaminated saliva, nasal, or aerosols (Wang et al., 2020; Sun et al., 2020) and presents cold-like symptoms in the early stages of infection, with a long incubation period of around two weeks. Although many strategies have been developed to prevent the transmission of SARS-CoV-2, prompt isolation of infected patients is still regarded as the most effective method (Bhadoria et al., 2020). However, the exclusion of asymptomatic viral carriers from diagnosis targets has contributed to its continued spread (Wang et al., 2020; Sun et al., 2020; Zhao et al., 2020).

Currently, SARS-CoV-2 detection primarily relies on nucleic acid amplification and serology-based antigen-binding assays (Zhu et al., 2020; Beig Parikhani et al., 2021; Ji et al., 2020). However, the reverse transcriptase-polymerase chain reaction requires a relatively long time (*i.e.*, a few hours) for complementary deoxyribonucleic acid (DNA) amplification including pre-/post-treatment, and the antigen-antibody interaction for SARS-CoV-2 has a low accuracy due to the high structural similarity of antigens within the same genus (Morales-Narváez et al., 2020; Niemz et al., 2011; Tai et al., 2020). Although several strategies for specific viral detection have been recently reported, for

* Corresponding author. Sensor System Research Center, Korea Institute of Science and Technology (KIST), Seoul, 02792, Republic of Korea.
** Corresponding author.
E-mail addresses: hssong@kist.re.kr (H.S. Song), mseo@kist.re.kr (M. Seo).
[1] These authors contributed equally to this work.

https://doi.org/10.1016/j.bios.2022.113981
Received 15 June 2021; Received in revised form 12 October 2021; Accepted 7 January 2022
Available online 14 January 2022

examples, the rolling circle replication (Yan et al., 2021; Yue et al., 2021), DNA methylation (Ganesh et al., 2020), electrochemical CRISPR (Bruch et al., 2019; Li et al., 2021), and chemiluminescence resonance energy transfer (Yan et al., 2020), the development of rapid diagnostic techniques based on sophisticated molecular structures is urgently required. For the case of SARS-CoV and SARS-CoV-2, it is well-known that both take advantage of the angiotensin-converting enzyme 2 (ACE2) receptor for host entry using spike (S) proteins in their membranes (Ji et al., 2020; Yan et al., 2020; Lan et al., 2020). Differences in their S protein sequences, especially in their receptor-binding domain (RBD), determine their structure, viral transmission, and neutralizing efficiency (Lan et al., 2020; Hoffmann et al., 2020; Krammer et al., 2020; Kim et al., 2021). For this reason, the S protein represents an ideal target for viral discrimination and subsequent vaccine and therapeutic development.

Metamaterial-based terahertz time-domain spectroscopy (THz-TDS) has recently attracted increasing attention, particularly in chemical and biomedical sensing applications (Fan et al., 2014; Choi et al., 2011; Yang et al., 2016; Gong et al., 2020). Due to its low photon energy irradiation (1 THz, which is equivalent to 4 meV), THz-TDS offers insight into the structural and dynamical characteristics of organic compounds and does not lead to ionization, radiative thermal excitation, or damage (Fan et al., 2014; Choi et al., 2011; Yang et al., 2016). It scans unique spectral features in the ultrabroad spectrum corresponding to vibrational/rotational modes (referred to as "fingerprints"), overall molecular motion, and phonon vibrations, especially in low frequencies ($\leq$100 cm^{-1}). These low-frequency vibrations contain information about hydrogen bonds, van der Waals forces, torsion, and hydrophobic interactions, which allow a deeper understanding of biological targets (*e.g.*, proteins, nucleosides, peptides, amino acids (AAs), and DNA) (Yang et al., 2016; Gong et al., 2020; Born et al., 2009; Janek et al., 2014). Furthermore, metamaterial-based sensing chips with elaborately designed structures at a subwavelength scale (λ/10−λ/10,000) have been developed to enhance the sensitivity and obtain the higher signal-to-noise (S/N) ratio in response to the intrinsically weak molecular absorption within the THz regime (Choi et al., 2011; Lee et al., 2020; Srivastava et al., 2019). These chips produce a specific resonance frequency (f_{res}) that is tunable by adjusting the geometric parameters of the antenna-type nanoslot structures. These advantages allow THz-TDS to effectively and rapidly probe and identify biomolecules with high structural similarity even at extremely low concentrations.

In this work, we developed nanoscale metamaterial-based THz-TDS for the detection and discrimination of peptides. The THz signals responsible for the low vibrational frequencies were employed to reveal the properties of individual components. Peptides derived from the S protein in SARS-CoV and SARS-CoV-2 were selected as viral model analytes. The selectivity and specificity of the proposed approach were experimentally and quantitatively examined using THz signals at f_{res} = 1.16, 1.64, and 2.07 THz that were strongly enhanced by the metamaterials. The effects of hydropathy and the net charge of the peptides on the THz features were also explored. In our THz-TDS system, data could be acquired within a few minutes with a sufficiently stable S/N ratio of 70 dB, thus it represents a new type of rapid and accurate sensing platform.

2. Experimental details

2.1. Materials

Given the sequence similarity of SARS-CoV and SARS-CoV-2, two pairs of peptides from the RBD of their S proteins were individually synthesized (Peptron, Daejeon, South Korea). These pairs were AA residue 427–446 (NIDATSTGNYNYKYRYLRHG; SCRBD-1) and residue 447–466 (KLRPFERDISNVPFSPDGKP; SCRBD-2) from SARS-CoV and residue 440–459 (NLDSKVGGNYNYLYRLFRKS; SC2RBD-1) and residue 460–479 (NLKPFERDISTEIYQAGSTP; SC2RBD-2) from SARS-CoV-2. Schematic information of genome and peptide sequences were taken from NCBI GenBank (accession codes MN908947 for human SARS-CoV-2 and AY278741 for human SARS-CoV). The structures of the SARS-CoV-based peptides (*i.e.*, SCRBD-1 and SCRBD-2) and those of the SARS-CoV-2-based peptides (*i.e.*, S protein, SC2RBD-1, and SC2RBD-2) were described using 6NB6 and 6XEY from the Protein Data Bank (PDB), respectively.

2.2. Fabrication of nanoslot arrays

Nanoslot arrays with a high aspect ratio to enhance the THz signal were fabricated based on a conventional semiconductor process. A six in un-doped silicon (Si) wafer with a high resistivity of $> 10^4$ Ω cm was cleaned using a piranha solution (H_2SO_4:H_2O_2 = 3:1) and a diluted hydrofluoric acid solution (HF:H_2O = 1:100). In order to improve the compatibility with biomolecules, a 300 nm-thick Si dioxide (SiO_2) layer was thermally deposited onto the wafer using a furnace. The nanoslot patterns were defined using photolithography, which was followed by metallization (Ti/Au; 10/150 nm) and a lift-off process.

2.3. THz-TDS measurements

A THz-TDS system in transmittance mode was designed based on the Ti:sapphire femtosecond laser with a center λ *of* 800 nm, a pulse width of 100 fs, and a repetition rate of 80 MHz. To take the measurements, a chamber environment containing a full THz beam path was sealed with purged dried air (relative humidity of less than 1%) to prevent the loss of the THz signal due to water vapor absorption. The THz electric (*E*)-field was derived from the 30-times-averaged time-domain waveforms, which were then converted into frequency-domain data using the fast Fourier transform. The transmittance ($T(\omega)$) was defined as, $T(\omega) = \left|E_{sample}(\omega)/E_{sub}(\omega)\right|^2$, where $E_{sample}(\omega)$ and $E_{sub}(\omega)$ are the *E*-field transmitted through the THz metamaterials with and without the peptides, respectively. To prepare the samples, each peptide was dissolved in deionized (DI) water at different concentrations (0.1, 0.5, and 1.0 mg/mL). DI water was chosen as the solvent to avoid a spectral shift occurring due to the competition between ions and the proteins. A 2 μl aliquot of the solution was dropped onto the surface of the THz metamaterials and then dried for 15 min in a vacuum.

2.4. Theoretical computations

The *E*-field profiles of the nanoslot metamaterials were theoretically investigated based on the finite element method (FEM) using an electromagnetic (EM) wave module in the commercial software package COMSOL Multiphysics. Details of the simulation parameters are provided in Table S1. The complex permittivity of the Au layer was extracted from the standard Drude model. Given the regular arrangement of the nanoslots, a periodic boundary condition (BC) was applied to the *x*- and *y*-directions. An active port BC at the top of the air domain was used to generate the incident THz wave while a passive port was employed at the bottom of the metamaterial model. A perfectly matched layer with a scattering BC that simulated the infinite free space was employed to pass light out of the domain without reflection.

3. Results and discussion

3.1. Characteristics of the peptide pairs

The strategy for sensing and discriminating the peptides from SARS-CoV and SARS-CoV-2 based on the THz metamaterial is illustrated in Fig. 1a. Both belong to the betacoronaviruses (β-CoV) within the coronaviridae, which is a family of enveloped, positive-sense, and single-stranded RNA viruses (*i.e.*, Baltimore class IV). They have significant structural similarity, with an 82% viral genome identity (Naqvi et al.,

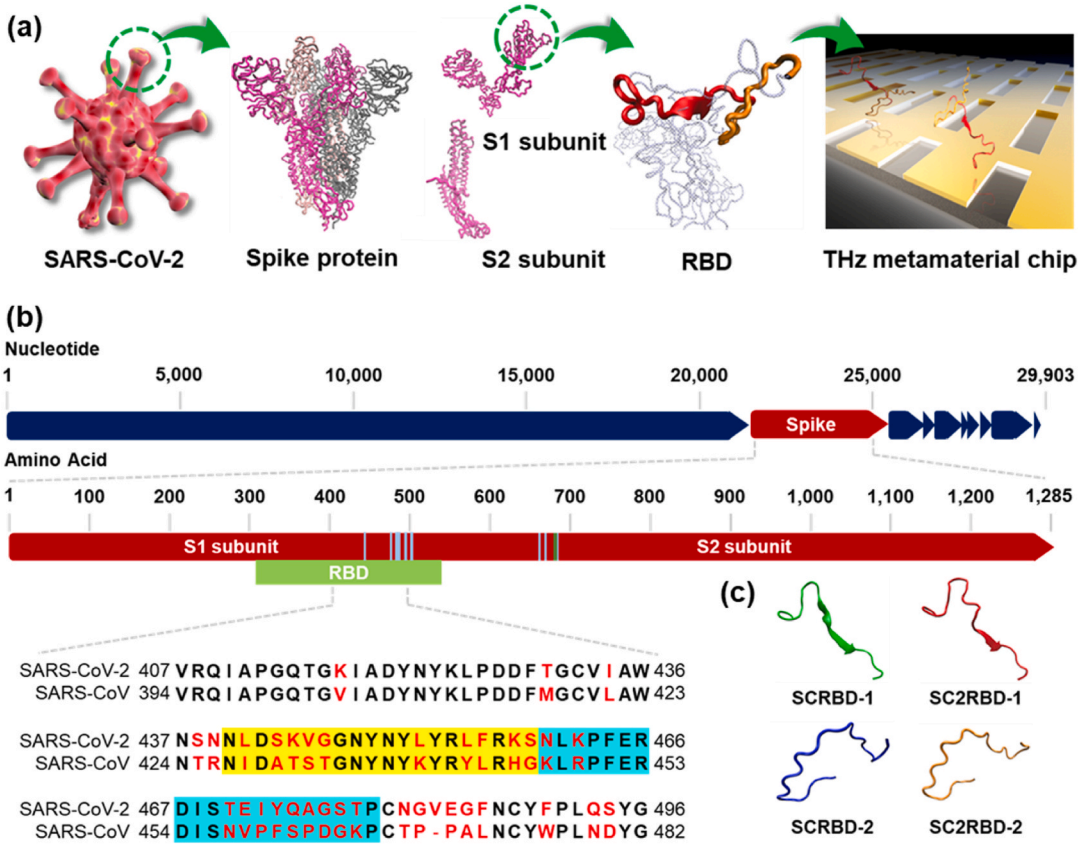

Fig. 1. (a) Schematic diagram of the detection and discrimination of SARS-CoV-2 and SARS-CoV using a THz metamaterial. (b) Features of the whole genome and AA sequence of SARS-CoV-2. The AA sequence in the RBD of SARS-CoV-2 and SARS-CoV are presented. The yellow region indicates SCRBD-1 and SC2RBD-1, and the blue region indicates SCRBD-2 and SC2RBD-2. (c) Crystal structure of SCRBD-1,2 (PDB ID: 6NB6) and SC2RBD-1,2 (PDB ID: 6XEY) used in THz-TDS sensing.

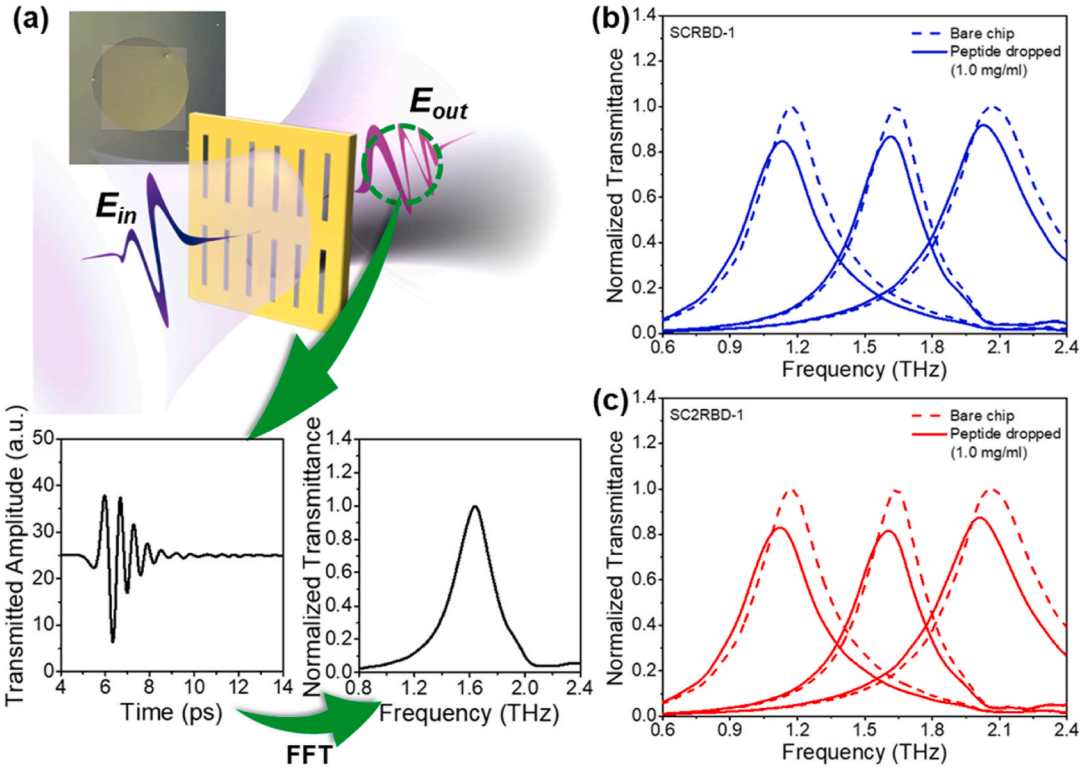

Fig. 2. (a) Sensing process for THz-TDS in transmittance mode. The signal obtained in the time domain was converted to data in the frequency domain using fast Fourier transform. Normalized THz spectra for (b) SCRBD-1 and (c) SC2RBD-1 at 1.0 mg/mL and f_{res} = 1.16, 1.64, and 2.07 THz are presented.

2020; Lu et al., 2020). Their RNA genome primarily encodes four proteins: the S protein, envelope protein, membrane protein, and nucleocapsid protein (Beig Parikhani et al., 2021; Ji et al., 2020; Tai et al., 2020; Krammer et al., 2020; Kim et al., 2021; Naqvi et al., 2020). The S protein, which is highly glycosylated trimeric membrane protein, consists of S1 and S2 subinits, mediating viral binding and membrane fusion, respectively. (Beig Parikhani et al., 2021; Tai et al., 2020; Yan et al., 2020; Lan et al., 2020; Kim et al., 2021). When the virus enters the host, the RBD in the S1 subunit plays a key role in the interaction with the ACE2 receptor. For their RBD, the highly similar sequences (approximately 73%) and secondary structures are observed (Fig. 1b and c) (Beig Parikhani et al., 2021; Ji et al., 2020; Wan et al., 2020). To determine their unique characteristics derived from their AA composition, two pairs of 20 AAs were selected from the RBD of SARS-CoV and SARS-CoV-2. In the comparison, the peptides were paired as SCRBD-1/SC2RBD-1 (yellow highlights) and the SCRBD-2/SC2RBD-2 (blue highlights).

3.2. THz responses to SCRBD-1 and SC2RBD-1

The fundamental mechanisms of the nanoslot structure are presented in Fig. 2a. For THz metamaterials, the geometric parameters of the nanoslots are crucial to the overall performance of the resulting sensing device. The length (l) of the slot is related to f_{res} based on the following equation (Lee et al., 2020):

$$f_{res} = c_0 \Big/ l\sqrt{2(n^2+1)}, \quad (1)$$

where c_0 is the speed of light and n is the refractive index of the substrate. In this study, l was 32, 40, and 60 μm, corresponding to a f_{res} of 2.07, 1.64, and 1.16 THz, respectively. The width (w) of the slot is associated with the trade-off relationship between sensitivity (*i.e.*, *E*-field enhancement) and the molecule-capturing volume. As w becomes narrower, THz field enhancement increases due to the funneling effect, while the volume containing the target molecules (*i.e.*, the optical hotspot and the active area) is reduced. To optimize this trade-off, w was set at 500 nm, as demonstrated by our previous studies (Lee et al., 2020, 2021; Seo et al., 2009). The distance between each slot was set at 40 and 10 μm along the transverse and longitudinal directions, respectively, to obtain highly resolute spectra smaller than the first Rayleigh minimum. To prevent the direct transmission of incident THz waves through the metal film, the thickness of the Au layer was set at 150 nm, which was much greater than its skin depth ($\delta\sim$ 73, 61, and 55 nm at 1.16, 1.64, and 2.07 THz, respectively). The highly resistive substrate maximized the S/N ratio due to an unaltered n ($n_{SiO2}\approx$ 1.96 and $n_{Si}\approx$ 3.41) and a low absorption coefficient (α) in the THz regime (0.5–2.5 THz). The transmitted signals in the time domain were obtained and consequently converted to the frequency domain using the fast Fourier transform.

To explore the THz-based optical responses to the S proteins of SARS-CoV and SARS-CoV-2, sensing chips with three different f_{res} (*i.e.*, 1.16, 1.64, and 2.07 THz) were employed. The optical characteristics of the peptides were evaluated based on the shifts in frequency ($\Delta f = f_{res}$-f) and changes in the transmittance ($\Delta T/T_0$) between the THz spectra with and without the peptide samples. Although the T and f_{res} of the nanoslot cannot be precisely calculated by the Fresnel equation, to be brief, the dominant factor affecting Δf is the effective refractive index (*i.e.*, n), while the absorption cross-section (*i.e.*, k) of the target has a strong influence on $\Delta T/T_0$ (Srivastava et al., 2019; Lee et al., 2021; Park et al., 2014). To determine the influence of AA composition on THz features, SCRBD-1 and SC2RBD-1 were analyzed. Their THz spectra for a concentration of 1.0 mg/mL averaged from multiple chips are presented in Fig. 2b and c. The differences in Δf and $\Delta T/T_0$ for SCRBD-1 and SC2RBD-1 were very small at f_{res} = 1.16 THz but they increased noticeably at a higher f_{res} (Table 1). These results indicate that peptides with similar secondary backbone structures can be classified using their unique THz fingerprints.

Table 1
THz responses for SCRBD-1 and SC2RBD-1 at 1.0 mg/ml and various f_{res} values.

	f_{res} = 1.16 THz		f_{res} = 1.64 THz		f_{res} = 2.07 THz	
peptide	Δf (THz)	ΔT/T$_0$ (%)	Δf (THz)	ΔT/T$_0$ (%)	Δf (THz)	ΔT/T$_0$ (%)
SCRBD-1	0.039	15.27	0.026	13.55	0.040	8.62
SC2RBD-1	0.043	16.47	0.040	16.48	0.053	13.39

At cryogenic temperatures, biosamples generally produce absorption features (α) that reflect the characteristics of the individual molecular components (Neu et al., 2019; Laman et al., 2008; Pan et al., 2017). With increasing environmental temperature, the transition from the thermally occupied states broadens and slightly shifts the molecular spectral features, leading to information of a lower resolution. In addition, large samples including proteins and peptides with relatively long segments demonstrate no significant optical features (Lee et al., 2017). In contrast, relatively short segments were employed in the present study, so the influence of major AA components on the THz spectra was able to be considered. For SCRBD-1 and SC2RBD-1, the leucine (Leu) and asparagine (Asn) were analyzed due to their prominent α features in the transmitted THz signals from a pellet mixed with high-density polyethylene, which is almost transparent in the THz regime (Supplementary Information). Prominent peaks were observed at 0.64, 0.82, 1.43, 1.64, and 2.11 THz for Leu and 1.63 and 2.20 THz for Asn, which is consistent with other reports (Nishizawa et al., 2006; Wang et al., 2009). Based on the major AA components, at 1.64 and 2.07 THz, the intrinsic α and corresponding $\Delta T/T_0$ of SC2RBD-1 may be higher than those of SCRBD-1. Thus, THz-TDS is able to discriminate between extremely small biomarkers (λ/10,000−λ/100,000) with high structural similarity, thus demonstrating its potential for use in practical bioassays.

3.3. Quantitative comparison of SCRBD-1 and SC2RBD-1

For effective and reliable early diagnosis, high sensitivity, a low limit of detection (LOD), and high reproducibility are required. To investigate those key parameters, quantitative analysis (0.1, 0.5, and 1.0 mg/mL) of SCRBD-1 and SC2RBD-1 was conducted (Fig. 3a–f). The average concentration-dependent Δf and $\Delta T/T_0$ for each f_{res} are summarized in Fig. 3g. For all concentrations, similar trends were observed. It was thus possible to distinguish SCRBD-1 and SC2RBD-1, which share similar secondary structures (Fig. 1b; part of the α-helix and β-strand), even at low concentrations. A highly linear relationship was observed with the concentration with correlation coefficients (R^2) of >98.4% and >98.6% for SCRBD-1 and SC2RBD-1, respectively, thus indicating the excellent quantitative sensitivity of THz-TDS. Accordingly, the LOD was estimated to be 0.1 mg/mL (*i.e.*, 41.7 μM).

The reproducibility of the THz signals was estimated using the standard deviation (SD) of multiple runs. SC2RBD-1 had a relatively large SD compared to that of SCRBD-1, which was related to their molecular distribution. One factor determining the SD is the isoelectric point (pI), which determines the net charge of peptides in relation to the pH of a solvent. Based on data from Thermofisher Scientific (https://www.thermofisher.com/kr/en/home.html), the pI was theoretically expected to be 9.8 and 10.2 for SCRBD-1 and SC2RBD-1, respectively, which is much higher than the pH of the solvent used in the present study (DI water; ~6.8), indicating that the peptides are positively charged (pI > pH). Thus, an attractive force between the peptides and the Au layer was induced. Consistent with this phenomenon, during the drying process, the surface of the peptide films was uniformly polymerized without notable deformations (Supplementary Information).

Another factor related to the SD is hydropathy. Hydrophilicity leads to more beneficial molecular solubility, dispersion, and distribution. Among biomolecules, the most typical hydrophilic interactions are hydrogen bonds and salt bridges (Lan et al., 2020). Polar and

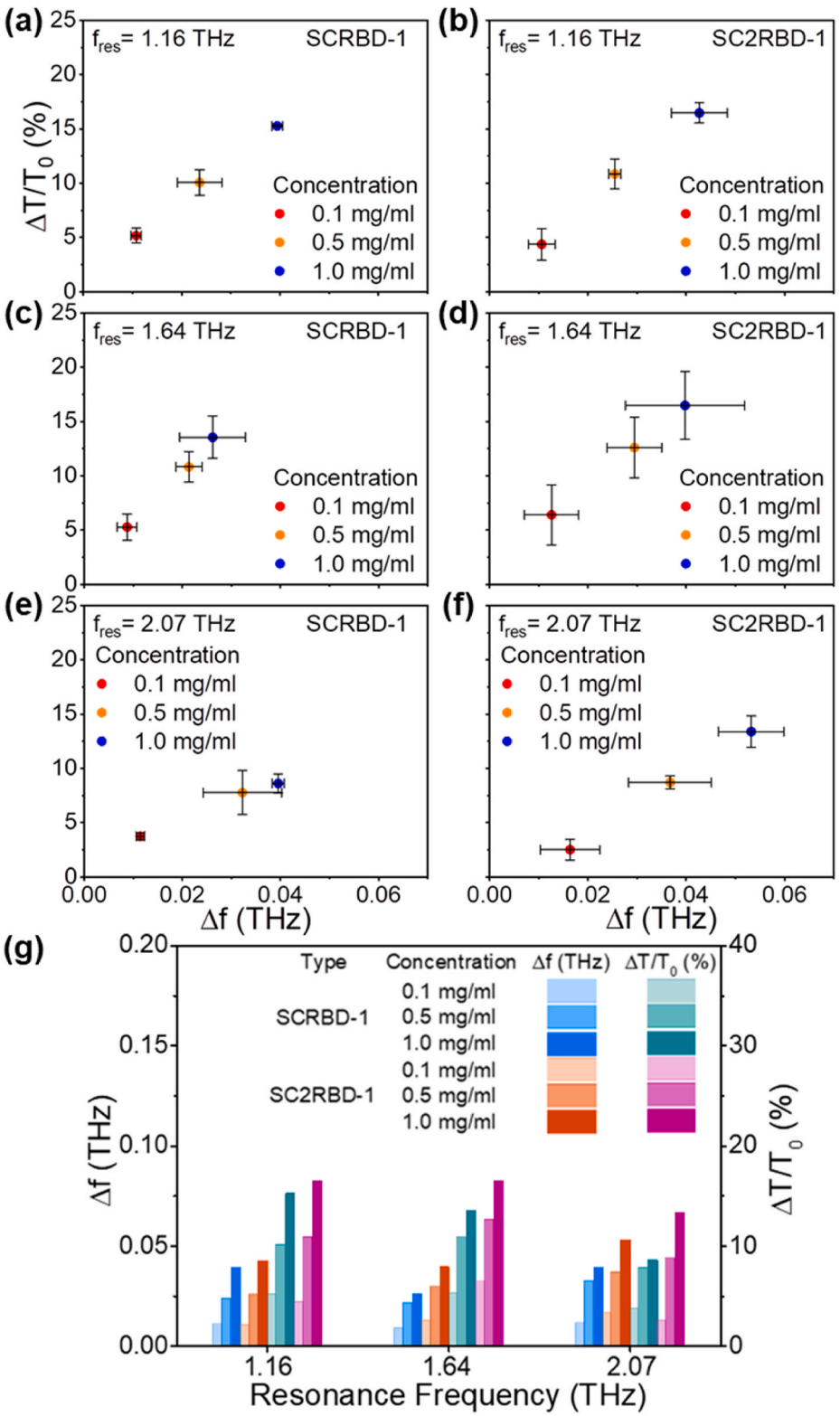

Fig. 3. Quantitative THz analysis for SCRBD-1 and SC2RBD-1 at f_{res}= (a,b) 1.16, (c,d) 1.64, and (e,f) 2.07 THz and (g) an overall summary.

amphipathic AAs readily form hydrogen bonds with other polar groups while charged AAs often participate in salt interactions (Lan et al., 2020, Mermut et al., 2006; Fernández-Carneado et al., 2004). It has been reported that there are 13 hydrogen bonds and 2 salt bridges at the SC2RBD/ACE2 interface and 13 hydrogen bonds and 3 salt bridges at the SCRBD/ACE2 interface (Lan et al., 2020; Lu et al., 2020; Wan et al., 2020). In particular, the highly hydrophilic Y and N are observed for SCRBD-1 (N427, N435, Y436, N437, Y438, Y440, and Y442) and SC2RBD-1 (N440, Y449, N450, Y451, N452, and Y453). To compare their wettability properties, the grand average of hydropathy (GRAVY) index, evaluated using the averaged Kyte-Doolittle scale, was calculated. A positive GRAVY value indicates hydrophobicity, while a negative value indicates hydrophilicity. The GRAVY index of SCRBD-1 and SC2RBD-1 was calculated to be −1.41 and −0.94, respectively. Due to

the surface tension across the slots, more hydrophilic components penetrate more efficiently into narrow regions, resulting in a lower SD.

3.4. Net charge effect on the THz signal

To investigate the effect of AA composition on the THz signal, 20 additional AAs with similar secondary structures were analyzed. The 20 AAs with the sequences of 447–466 (SCRBD-2) and 460–479 (SC2RBD-2) were selected, respectively, representing the κ-helix (also known as polyproline II, PPII). The dominant AAs within the κ-helix are proline, which is characterized by the absence of H-donor atoms in its cyclic side chain, and glycine (Fernández-Carneado et al., 2004). These residues are major AA components in both peptides. For SCRBD-2 and SC2RBD-2, the f_{res} and concentration-dependent THz signals were characterized

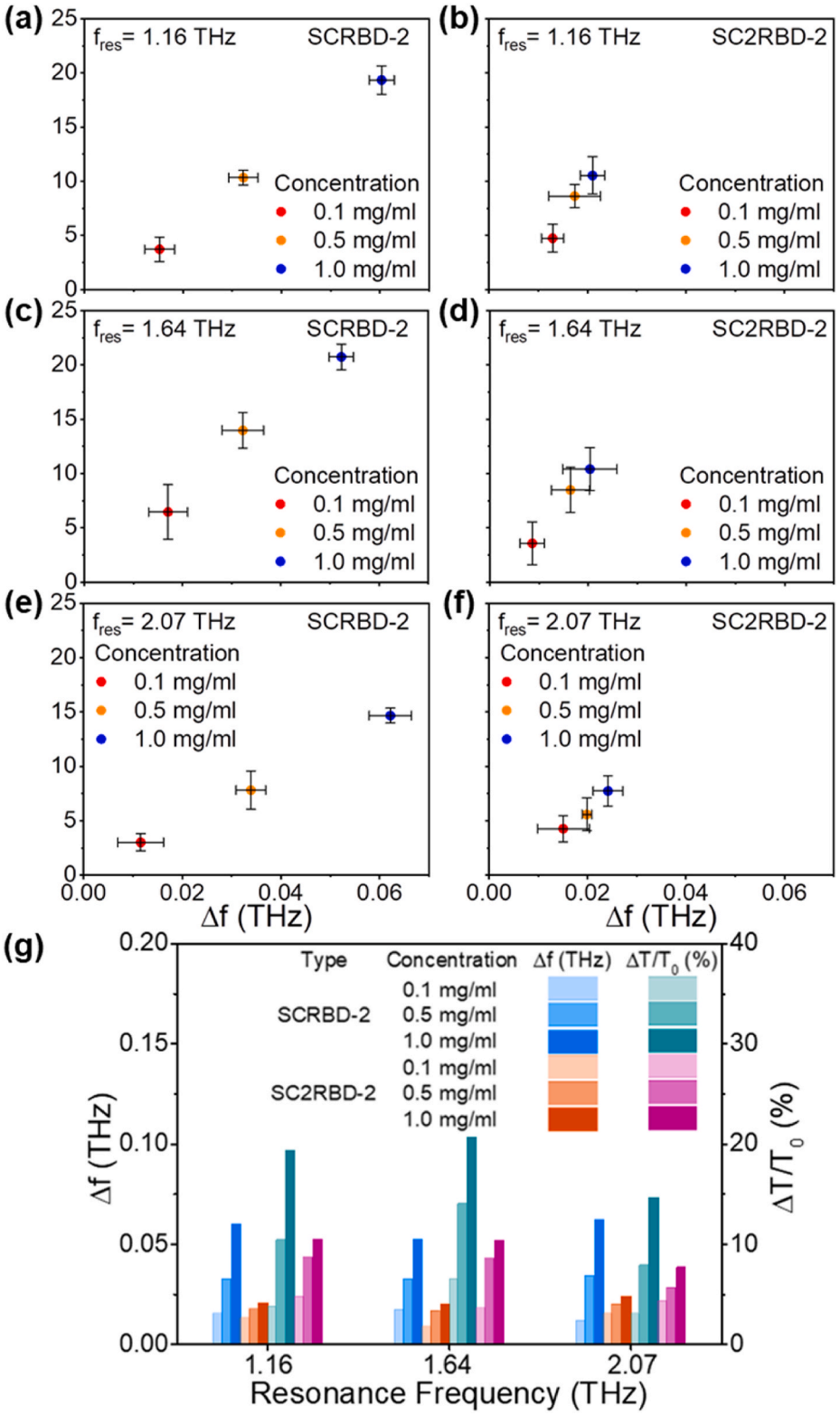

Fig. 4. Quantitative THz analysis for SCRBD-2 and SC2RBD-2 at f_{res}= (a,b) 1.16, (c,d) 1.64, and (e,f) 2.07 THz and (g) an overall summary.

(Fig. 4a–f) and their averages are summarized in Fig. 4g. At all f_{res}, high linearity was observed in the relationship with the concentration, with an R^2 of >0.98 and > 0.94 for SCRBD-2 and SC2RBD-2, respectively. For all f_{res} and at 1 mg/mL, prominent increases THz spectra were observed ($\Delta f \geq 0.05$ THz and $\Delta T/T_0 \geq 15\%$) for SCRBD-2, while a dramatic decrease was observed for SC2RBD-2 ($\Delta f < 0.03$ THz and $\Delta T/T_0 < 13\%$), despite its similar κ-helix structure. Thus, SCRBD-2 and SC2RBD-2 were successfully discriminated using the THz spectra, though the mechanisms somewhat differ from the case for SCRBD-1 and SC2RBD-1.

This large discrepancy can be explained based on the probability of the molecules being captured by the active regions, as illustrated by the following equation (Lee et al., 2021; Park et al., 2014):

$$\frac{\Delta f}{f_0} \propto \frac{N_s(\varepsilon_{AA} - \varepsilon_{air})}{\varepsilon_{eff}}, \quad (2)$$

where N_s is the number of AAs in the nanoslot gap and ε_{AA}, ε_{air}, and ε_{eff} are the permittivity of the AA, the air, and the gap without AAs, respectively. In Eq. (2), N_s is the critical variable determining Δf; thus, the results indicate that significantly fewer SC2RBD-2 molecules were trapped by the slots compared to SCRBD-2. This can be ascribed to the electrostatic repulsive force between SC2RBD-2 and the Au layer. The theoretically expected pI value was about 9.9 and 4.4 for SCRBD-2 and SC2RBD-2, respectively. In this case, both the Au layer filled with numerous free electrons and SC2RBD-2 dissolved in DI water (pI < pH) were negatively charged, and consequently, they repelled one another. This interaction hindered the efficient molecular adsorption and the sensing performance of the metamaterial. For this reason, it is speculated that an inhomogeneous SC2RBD-2 distribution was created when the droplet was placed on the metamaterial. Once it had completely dried, the formation of an irregular film with crack lines was observed (Supplementary Information). This non-uniform distribution of SC2RBD-2 was also consistent with its relatively large SD when compared to that of SCRBD-2.

4. Conclusions

We successfully compared and analyzed the peptides in the RBD of SARS-CoV-2 and SARS-CoV, which share highly similar secondary structures. Using THz metamaterials (f_{res} = 1.16, 1.64, and 2.07 THz), the spectral fingerprints at low frequencies of the peptides were measured. These fingerprints originated from a variety of structural properties, including the peptides themselves, individual AAs, and hydrogen bonds. The variation and SD of the THz signals (*i.e.*, Δf and $\Delta T/T_0$) were also analyzed based on the hydropathy and net charge of the peptides. For SCRBD-1 and SC2RBD-1, which share similar secondary structures (part of the α-helix and β-strand), the hydrophilic and positively charged peptides led to more effective molecular capture and higher film uniformity. The spectral differences at f_{res} = 1.64 and 2.07 THz were attributed to the number of major AAs (*i.e.*, Leu and Asn), which have strong intrinsic absorption peaks at the measured frequencies. On the other hand, for SCRBD-2 and SC2RBD-2, which share the κ-helix, significant differences in the signals were observed. The repulsive forces between the negatively charged SC2RBD-2 and the metamaterial disrupted effective molecular detection. Based on quantitative analysis, the LOD for all of the peptides was estimated to be 0.1 mg/mL (41.7 μM). Taken together, these results demonstrate the validity of the proposed approach to the detection and classification of biomolecules, even for those within the same genus, at the peptide level. Moreover, the THz system with fast acquisition and high S/N ratio contributed to the rapid trace of molecules within a few minute. Therefore, metamaterial-based THz-TDS analytic tools show great promise for point-of-care and label-free diagnosis in practical applications.

Declaration of competing interest

The authors declare that they have no known competing financial interests or personal relationships that could have appeared to influence the work reported in this paper.

Acknowledgements

This work was supported in part by KIST intramural grants (2E31721 and 2E31821), KU-KIST school project, and National Research Foundation of Korea (NRF) (NRF-2020R1A2C2007077 and 2021R1F1A1063877, and the Global Frontier Program CAMM-2019M3A6B3030638).

Appendix A. Supplementary data

Supplementary data to this article can be found online at https://doi.org/10.1016/j.bios.2022.113981.

References

Beig Parikhani, A., Bazaz, M., Bamehr, H., Fereshteh, S., Amiri, S., Salehi-Vaziri, M., Arashkia, A., Azadmanesh, K., 2021. The inclusive review on SARS-CoV-2 biology, epidemiology, diagnosis, and potential management options. Curr. Microbiol. 78, 1099–1114.
Bhadoria, A.S., Gawande, K., Sharma, R., Mohapatra, A., Kant, R., 2020. Institutional versus Home Isolation to Curb the COVID-19 Outbreak, vol. 396, pp. 1631–1632, 10263.
Born, B., Weingärtner, H., Bründermann, E., Havenith, M., 2009. Solvation dynamics of model peptides probed by terahertz spectroscopy. Observation of the onset of collective network motions. J. Am. Chem. Soc. 131 (10), 3752–3755.
Bruch, R., Baaske, J., Chatelle, C., Meirich, M., Madlener, S., Weber, W., Dincer, C., Urban, G.A., 2019. CRISPR/Cas13a-Powered electrochemical microfluidic biosensor for nucleic acid amplification-free miRNA diagnostics. Adv. Mater. 31, 1905311.
Choi, M., Lee, S.H., Kim, Y., Kang, S.B., Shin, J., Kwak, M.H., Kang, K.-Y., Lee, Y.-H., Park, N., Min, B., 2011. A terahertz metamaterial with unnaturally high refractive index. Nature 470, 369–373.
Fan, S., He, Y., Ung, B.S., Pickwell-MacPherson, E., 2014. The growth of biomedical terahertz research. J. Phys. D Appl. Phys. 47 (37), 374009.
Fernández-Carneado, J., Kogan, M.J., Castel, S., Giralt, E., 2004. Potential peptide carriers: amphipathic proline-rich peptides derived from the N-terminal domain of γ-zein. Angew. Chem. Int. Ed. 43 (14), 1811–1814.
Ganesh, S., Venkatakrishnan, K., Tan, Bo, 2020. Quantum scale organic semiconductors for SERS detection of DNA methylation and gene expression. Nat. Commun. 11, 1135.
Gong, A., Qiu, Y., Chen, X., Zhao, Z., Xia, L., Shao, Y., 2020. Biomedical applications of terahertz technology. Appl. Spectrosc. Rev. 55 (5), 418–438.
Hoffmann, M., Kleine-Weber, H., Schroeder, S., Krüger, N., Herrler, T., Erichsen, S., Schiergens, T.S., Herrler, G., Wu, N.-H., Nitsche, A., Müller, M.A., Drosten, C., Pöhlmann, S., 2020. SARS-CoV-2 cell entry depends on ACE2 and TMPRSS2 and is blocked by a clinically proven protease inhibitor. Cell 181 (2), 271–280.
Janek, M., Zich, D., Naftaly, M., 2014. Terahertz time-domain spectroscopy response of amines and amino acids intercalated smectites in far-infrared region. Mater. Chem. Phys. 145 (3), 278–287.
Ji, T., Liu, Z., Wang, G., Guo, X., Akbar khan, S., Lai, C., Chen, H., Huang, S., Xia, S., Chen, B., Jia, H., Chen, Y., Zhou, Q., 2020. Detection of COVID-19: a review of the current literature and future perspectives. Biosens. Bioelectron. 166, 112455.
Kim, Y.J., Lee, M.H., Lee, S.-R., Chung, H.-Y., Kim, K., Lee, T.G., Kim, D.Y., 2021. Neutralizing human antibodies against severe acute respiratory syndrome coronavirus 2 isolated from a human synthetic fab phage display library. Int. J. Mol. Sci. 22 (4), 1913.
Krammer, F., 2020. SARS-CoV-2 vaccines in development. Nature 586, 516–527.
Laman, N., Harsha, S.S., Grischkowsky, D., Melinger, J.S., 2008. High-resolution waveguide THz spectroscopy of biological molecules. Biophys. J. 94 (3), 1010–1020.
Lan, J., Ge, J., Yu, J., Shan, S., Zhou, H., Fan, S., Zhang, Q., Shi, X., Wang, Q., Zhang, L., Wang, X., 2020. Structure of the SARS-CoV-2 spike receptor-binding domain bound to the ACE2 receptor. Nature 581, 215–220.
Lee, D.-K., Kang, J.-H., Kwon, J., Lee, J.-S., Lee, S., Woo, D.H., Kim, J.H., Song, C.-S., Park, Q.-H., Seo, M., 2017. Nano metamaterials for ultrasensitive Terahertz biosensing. Sci. Rep. 7, 8146.
Lee, S.-H., Shin, S., Roh, Y., Oh, S.J., Lee, S.H., Song, H.S., Ryu, Y.-S., Kim, Y.K., Seo, M., 2020. Label-free brain tissue imaging using large-area terahertz metamaterials. Biosens. Bioelectron. 170, 112663.
Lee, S.H., Roh, Y., Lee, S.-H., Ryu, Y.-S., Ju, B.-K., Seo, M., 2021. Direct comparison with terahertz metamaterials and surface-enhanced Raman scattering in a molecular-specific sensing performance. Opt Express 29 (1), 12–23.
Li, Z., Ding, X., Yin, K., Xu, Z., Cooper, K., Liu, C., 2021. Electric field-enhanced electrochemical CRISPR biosensor for DNA detection. Biosens. Bioelectron. 192, 113498.

Lu, R., Zhao, X., Li, J., Niu, P., Yang, B., Wu, H., Wang, W., Song, H., Huang, B., Zhu, N., Bi, Y., Ma, X., Zhan, F., Wang, L., Hu, T., Zhou, H., Hu, Z., Zhou, W., Zhao, L., Chen, J., Meng, Y., Wang, J., Lin, Y., Yuan, J., Xie, Z., Ma, J., Liu, W.J., Wang, D., Xu, W., Holmes, E.C., Gao, G.F., Wu, G., Chen, W., Shi, W., Tan, W., 2020. Genomic characterisation and epidemiology of 2019 novel coronavirus: implications for virus origins and receptor binding. Lancet 395 (10224), 565–574.

Mermut, O., Phillips, D.C., York, R.L., McCrea, K.R., Ward, R.S., Somorjai, G.A., 2006. In situ adsorption studies of a 14-amino acid leucine-lysine peptide onto hydrophobic polystyrene and hydrophilic silica surfaces using quartz crystal microbalance, atomic force microscopy, and sum frequency generation vibrational spectroscopy. J. Am. Chem. Soc. 128, 3598–3607.

Morales-Narváez, E., Dincer, C., 2020. The impact of biosensing in a pandemic outbreak: COVID-19. Biosens. Bioelectron. 163, 112274.

Naqvi, A.A.T., Fatima, K., Mohammad, T., Fatima, U., Singh, I.K., Singh, A., Atif, S.M., Hariprasad, G., Hasan, G.M., Hassan, MdI., 2020. Insights into SARS-CoV-2 genome, structure, evolution, pathogenesis and therapies: structural genomics approach. BBA-Mol. Basis Dis. 1866 (10), 165878.

Neu, J., Stone, E.A., Spies, J.A., Storch, G., Hatano, A.S., Mercado, B.Q., Miller, S.J., Schmuttenmaer, C.A., 2019. Terahertz spectroscopy of tetrameric peptides. J. Phys. Chem. Lett. 10 (10), 2624–2628.

Niemz, A., Ferguson, T.M., Boyle, D.S., 2011. Point-of-care nucleic acid testing for infectious diseases. Trends Biotechnol. 29 (5), 240–250.

Nishizawa, J., Sasaki, T., Suto, K., Tanabe, T., Yoshida, T., Kimura, T., Saito, K., 2006. Frequency-tunable terahertz-wave generation from GaP using Cr: forsterite lasers. Int. J. Infrared Millimet. Waves 27 (6), 779–789.

Pan, T., Li, S., Zou, T., Yu, Z., Zhang, B., Wang, C., Zhang, J., He, M., Zhao, H., 2017. Terahertz spectra of L-phenylalanine and its monohydrate. Spectrochim. Acta 178, 19–23.

Park, S.J., Hong, J.T., Choi, S.J., Kim, H.S., Park, W.K., Han, S.T., Park, J.Y., Lee, S., Kim, D.S., Ahn, Y.H., 2014. Detection of microorganisms using terahertz metamaterials. Sci. Rep. 4, 4988.

Seo, M.A., Park, H.R., Koo, S.M., Park, D.J., Kang, J.H., Suwal, O.K., Choi, S.S., Planken, P.C.M., Park, G.S., Park, N.K., Park, Q.H., Kim, D.S., 2009. Terahertz field enhancement by a metallic nano slit operating beyond the skin-depth limit. Nat. Photonics 3, 152–156.

Srivastava, Y.K., Ako, R.T., Gupta, M., Bhaskaran, M., Sriram, S., Singh, R., 2019. Terahertz sensing of 7 nm dielectric film with bound states in the continuum metasurfaces. Appl. Phys. Lett. 115, 151105.

Sun, J., He, W.-T., Wang, L., Lai, A., Ji, X., Zhai, X., Li, G., Suchard, M.A., Tian, J., Zhou, J., Veit, M., Su, S., 2020. COVID-19: epidemiology, evolution, and cross-disciplinary perspectives. Trends Mol. Med. 26 (5), 483–495.

Tai, W., He, L., Zhang, X., Pu, J., Voronin, D., Jiang, S., Zhou, Y., Du, L., 2020. Characterization of the receptor-binding domain (RBD) of 2019 novel coronavirus: implication for development of RBD protein as a viral attachment inhibitor and vaccine. Cell. Mol. Immunol. 17, 613–620.

Wan, Y., Shang, J., Graham, R., Baric, R.S., Li, F., 2020. Receptor recognition by the novel coronavirus from wuhan: an analysis based on decade-long structural studies of SARS coronavirus. J. Virol. 94 (7), e00127-20.

Wang, W.-N., Li, H.-Q., Zhang, Y., Zhang, C.-L., 2009. Correlations between terahertz spectra and molecular structures of 20 standard α-amino acids. Acta Phys. Chim. Sin. 25 (10), 2074–2079.

Wang, C., Horby, P.W., Hayden, F.G., Gao, G.F., 2020. A novel coronavirus outbreak of global health concern. Lancet 395 (10223), 470–473.

Yan, Y., Wang, X., Hai, X., Song, W., Ding, C., Cao, J., Bi, S., 2020a. Chemiluminescence resonance energy transfer: from mechanisms to analytical applications. TrAC Trends Anal. Chem. (Reference Ed.) 123, 115755.

Yan, R., Zhang, Y., Li, Y., Xia, L., Guo, Y., Zhou, Q., 2020b. Structural basis for the recognition of SARS-CoV-2 by full-length human ACE2. Science 367 (6485), 1444–1448.

Yan, Y., Qiao, Z., Hai, X., Song, W., Bi, S., 2021. Versatile electrochemical biosensor based on bi-enzyme cascade biocatalysis spatially regulated by DNA architecture. Biosens. Bioelectron. 174, 112827.

Yang, X., Zhao, X., Yang, K., Liu, Y., Liu, Y., Fu, W., Luo, Y., 2016. Biomedical applications of terahertz spectroscopy and imaging. Trends Biotechnol. 34 (10), 810–824.

Yue, S., Li, Y., Qiao, Z., Song, W., Bi, S., 2021. Rolling circle replication for biosensing, bioimaging, and biomedicine. Trends Biotechnol. https://doi.org/10.1016/j.tibtech.2021.02.007 (in press).

Zhao, H., Lu, X., Deng, Y., Tang, Y., Lu, J., 2020. COVID-19: asymptomatic carrier transmission is an underestimated problem. Epidemiol. Infect. 148, 1–3.

Zhu, N., Zhang, D., Wang, W., Li, X., Yang, B., Song, J., Zhao, X., Huang, B., Shi, W., Lu, R., Niu, P., Zhan, F., Ma, X., Wang, D., Xu, W., Wu, G., Gao, G.F., Tan, W., 2020. A novel coronavirus from patients with pneumonia in China, 2019. N. Engl. J. Med. 382, 727–733.